Constraints on dark matter annihilation from CMB observations before Planck

Laura Lopez-Honorez[1], Olga Mena[2], Sergio Palomares-Ruiz[2,3] and Aaron C. Vincent[2]

[1] *Theoretische Natuurkunde, Vrije Universiteit Brussel and The
International Solvay Institutes Pleinlaan 2, B-1050 Brussels, Belgium*
[2] *Instituto de Física Corpuscular (IFIC), CSIC-Universitat de València,
Apartado de Correos 22085, E-46071 Valencia, Spain and*
[3] *Centro de Física Teórica de Partículas (CFTP), Instituto Superior Técnico,
Universidade Técnica de Lisboa, Av. Rovisco Pais 1, 1049-001 Lisboa, Portugal*
(Dated: September 13, 2013)

We compute the bounds on the dark matter (DM) annihilation cross section using the most recent Cosmic Microwave Background measurements from WMAP9, SPT'11 and ACT'10. We consider DM with mass in the MeV–TeV range annihilating 100% into either an e^+e^- or a $\mu^+\mu^-$ pair. We consider a realistic energy deposition model, which includes the dependence on the redshift, DM mass and annihilation channel. We exclude the canonical thermal relic abundance cross section ($\langle\sigma v\rangle = 3\times10^{-26}\mathrm{cm}^3\mathrm{s}^{-1}$) for DM masses below 30 GeV and 15 GeV for the e^+e^- and $\mu^+\mu^-$ channels, respectively. *A priori*, DM annihilating in halos could also modify the reionization history of the Universe at late times. We implement a realistic halo model taken from results of state–of–the–art N–body simulations and consider a mixed reionization mechanism, consisting on reionization from DM as well as from first stars. We find that the constraints on DM annihilation remain unchanged, even when large uncertainties on the halo model parameters are considered.

I. INTRODUCTION

The cosmic microwave background (CMB) radiation not only encodes information about the early universe until the epoch of recombination, but also about the integrated history of the intergalactic medium (IGM) between the surface of last scattering and the present. At early times, energy released into the IGM by dark matter (DM) annihilation affects the recombination process, increasing the ionization fraction and broadening the last scattering surface. At late times, annihilating DM in halos could also modify the reionization mechanism of the Universe. Therefore, DM annihilations generally alter the thermal history of the Universe, leading to observable changes in CMB temperature and polarization spectra [1–29] and to marginally observable effects in the CMB bispectrum [30].

New CMB data have recently become available. The Wilkinson Microwave Anisotropy Probe (WMAP) collaboration has made publicly available their final nine–year data release [31]. The South Pole Telescope (SPT) collaboration has released their measurements of 2540 deg^2 of sky, providing the CMB temperature anisotropy power over the multipole range $650 < \ell < 3000$ [32, 33], in the region from the third to the ninth acoustic peak. Finally, the Atacama Cosmology Telescope collaboration (ACT) has also released new measurements of the CMB damping tail [34].

In this work, we compute the constraints from these recent CMB measurements on annihilating DM particles with masses ranging from 1 MeV to 1 TeV, in combination with Baryon Acoustic Oscillation (BAO) data and Hubble Space Telescope (HST) measurements of the Hubble constant. Since ACT and SPT high multipole CMB measurements seem to disagree on the value of several cosmological parameters such as the effective number of relativistic species, the lensing potential, the neutrino masses and the properties of the dark radiation background [35–37], we analyze these two data sets separately.

We focus on purely leptonic annihilation channels, as e^+e^- and $\mu^+\mu^-$. Whereas in the case of the former channel very efficient energy injection into the IGM would occur, in the case of the latter an important part of the energy from DM annihilations would be "lost" in the form of neutrinos. Let us note that constraints on DM annihilating into nearly all other[1] two–particle SM final states should fall between the bounds obtained for $\mu^+\mu^-$ and e^+e^-. These channels are also partly motivated by recent explorations of astroparticle "anomalies", which point to a significant fraction of positrons above the expected background. The annihilation of leptophilic DM has been a candidate explanation for these anomalies, which include the positron fraction excess observed by PAMELA and Fermi above 10 GeV [38–49], the strong 511 keV signal from the galactic center seen most recently by the INTEGRAL/SPI experiment [50–62], and the large isotropic radio signal below 10 GHz observed by ARCADE [63–68].

We therefore explore here DM annihilations into either pure e^+e^- or pure $\mu^+\mu^-$ final states, using a realistic redshift– and DM mass–dependent model of energy injection into the IGM. We address the impact of DM annihilations through the epochs of recombination and reionization until today, considering a realistic halo formation model, and compute the constraints on the DM mass and annihilation cross section from the latest available cosmological data.

---

[1] Constraints from $\chi\chi \to \tau^+\tau^-$ channel are only slightly stronger than the constraints on $\chi\chi \to \mu^+\mu^-$ (see, e.g., Ref. [28]).

We begin by very briefly summarizing the theory of DM annihilation and its impact on CMB photons, before presenting our methods and results. Thus, in Section II, we explicitly show the parametrization of the energy injection and deposition from DM annihilation, including the enhancement due to halo formation. Section III summarizes the cosmological signatures of extra injected energy into the IGM. In Section IV we provide the details of our analysis, and finally give the results of our work in Section IV B. Details of the DM annihilation spectra are presented in Appendix A and the parametrization of the contribution from halos is given in Appendix B.

II. ENERGY DEPOSITION

In the following, we carefully distinguish between *injected* energy, defined as the energy liberated by DM annihilations, and *deposited* energy, which corresponds to the energy that actually goes into heating and ionization of the IGM. The annihilation of DM particles in the uniform density field of DM gives rise to an injection power into the IGM per unit volume at redshift z given by

$$\left(\frac{\mathrm{d}E}{\mathrm{d}V\mathrm{d}t}\right)_{\mathrm{injected}} = (1+z)^6(\Omega_{\mathrm{DM},0}\rho_{c,0})^2\zeta\frac{\langle\sigma v\rangle}{m_\chi} \, , \tag{1}$$

where $\Omega_{\mathrm{DM},0}$ is the present DM abundance, $\rho_{c,0}$ is the critical density today and $\langle\sigma v\rangle$ is the thermally–averaged DM annihilation cross section. If DM particles and antiparticles are identical ζ, the counting factor, is $\zeta = 1$ (which we will use in this work), and $\zeta = 1/2$ otherwise. If all the DM energy went into reheating the IGM, Eq. (1) would also correspond to the *deposited* energy. However, there are two factors which affect the efficiency of this process: 1) creation of "invisible" products, such as neutrinos as daughter particles; and 2) the free–streaming of electrons and photons from their creation until their energy is completely deposited into the IGM via photoionization, Coulomb scattering, Compton processes, bremsstrahlung and recombination. If this deposition is not complete, whatever remains would contribute to the present isotropic radiation background. Process 1) depends on the annihilation model, whereas process 2) depends on density and redshift, and is completely specified by the history of the IGM [7, 14, 19, 23, 26]. It is therefore convenient to parametrize the deposited energy as [14, 26]

$$\left(\frac{\mathrm{d}E}{\mathrm{d}t\mathrm{d}V}\right)_{\mathrm{deposited}} = f(z,m_\chi)\left(\frac{\mathrm{d}E}{\mathrm{d}t\mathrm{d}V}\right)_{\mathrm{injected}} \, , \tag{2}$$

so that all the z–dependence is in the factor $f(z,m_\chi)(1+z)^6$, where $f(z,m_\chi)$ represents the fraction of the injected energy by annihilations of DM particles with mass m_χ which is deposited into the IGM at redshift z. This efficiency factor[2] is defined as [26]

$$f(z,m_\chi) = \frac{H(z)}{(1+z)^3\sum_i\int\mathrm{d}E\,E\,\frac{\mathrm{d}N_i(E,m_\chi)}{\mathrm{d}E}}\sum_i\int\mathrm{d}z'\frac{(1+z')^2}{H(z')}\int\mathrm{d}E\,T_i(z',z,E)\,E\,\frac{\mathrm{d}N(E,m_\chi)}{\mathrm{d}E} \, . \tag{3}$$

The function $T_i(z',z,E)$ encodes the efficiency with which a photon ($i = \gamma$) or an electron/positron ($i = e^\pm$) injected at redshift z' and with energy E is deposited into the IGM at redshift z. The factors of $(1+z')$ in the integral are due to: the DM annihilation rate which goes as $n_{\mathrm{DM}}^2 \propto (1+z')^6$, the volume element $\mathrm{d}V$ which is proportional to $(1+z')^{-3}$, and the conversion from injection per unit time to injection per unit redshift, $\mathrm{d}t = -\mathrm{d}\ln(1+z')/H(z')$. The spectrum of injected particles, dN/dE, depends on the DM mass m_χ and on the annihilation channel. The denominator of Eq. (3) ensures that $f(z,m_\chi)$ is properly normalized to Eq. (1). The transfer function $T(z',z,E)$ was computed by several authors [14, 19, 23, 26] and has been tabulated and made public[3] by Slatyer [26].

It is interesting to note that the energy deposition efficiency can be larger than one for certain values of the DM mass. This is because particles injected into the "transparency window", $10^6\,\mathrm{eV} \lesssim E \lesssim 10^{12}\,\mathrm{eV}$, may propagate freely [1, 4, 14] until they are finally redshifted to energies low enough to efficiently Compton–scatter. This appears as an "extra" source of energy at lower z than one would not expect in the on–the–spot approximation, where energy deposition is taken to be instantaneous[4]. For practical reasons, we define below an effective energy deposition efficiency f_{eff} which depends on the DM mass.

---

[2] Our $f(z,m_\chi)$ is identical to the $f(z)$ defined by Ref. [26]. We have made the m_χ dependence explicit for clarity.
[3] http://nebel.rc.fas.harvard.edu/epsilon/
[4] The on–the–spot approximation, used in several previous analyses [1–6, 9, 13], is recovered with $T(z',z,E) = f\,\delta\left(\ln(1+z') - \ln(1+z)\right)$, where f is a constant efficiency factor, formally different from our f_{eff} defined below.

A. Inclusion of DM halos

Since the injection power from DM annihilation goes as n_{DM}^2, the enhancement due to the DM number density at late times by the formation and collapse of bound structures can provide a significant enhancement to the rate of injected energy. In order to compute the halo contribution, the halo mass function $\mathrm{d}n_{\mathrm{halo}}/\mathrm{d}M$ is required to specify the number of halos as a function of the halo mass M and redshift z. Some works [10, 11, 16, 17, 24] have used the analytic Press–Schechter spherical collapse model [69], whereas others [12, 15, 20, 22, 70] have considered the Sheth–Tormen ellipsoidal model [71]. In this work we follow a fully numerical approach by using the results of N–body simulations to obtain the halo mass function [72] and take the relation of the concentration parameter to the halo mass from Ref. [73], which we implement to obtain the single halo contribution assuming a Navarro, Frenk and White (NFW) DM density profile [74]. We provide the details of the used inputs, as well as some useful analytical parametrizations, in Appendix B. The energy injected into the IGM by DM annihilation in halos at redshift z is given by

$$\left(\frac{\mathrm{d}E}{\mathrm{d}V\mathrm{d}t}\right)_{\mathrm{halo,injected}} = \zeta \, \frac{\langle\sigma v\rangle}{m_\chi} \times \int_{M_{\mathrm{min}}}^{\infty} \mathrm{d}M \frac{\mathrm{d}n_{\mathrm{halo}}(M,z)}{\mathrm{d}M} \int_0^{r_\Delta} \mathrm{d}r \, 4\pi r^2 \, \rho_{\mathrm{halo}}^2(r) \; , \tag{4}$$

where the second integral represents the single halo contribution and the first integral parametrizes the weighted sum over all halos. The density profile of a DM spherical halo of mass M, radius r_Δ and concentration parameter $c_\Delta(M,z)$ is $\rho_{\mathrm{halo}}(r)$. In this work we use $\Delta = 200$. These quantities are defined so that $M = 4\pi/3 \, r_\Delta^3 \, \Delta \, \rho_{\mathrm{c}}(z)$. As for the lower limit of integration in the first integral, it has been shown that the two main damping processes that generate a exponential cutoff in the power spectrum are the free–streaming of DM particles from high to low density regions [75] and the effect of acoustic oscillations in the cosmic bath [76, 77]. These processes depend on the particle physics and cosmological model and hence the minimum halo mass M_{min} is a very model dependent quantity that can vary from $M_{\mathrm{min}} = 10^{-4} M_\odot$ to $M_{\mathrm{min}} = 10^{-11} M_\odot$ [78–80]. Observational probes of these microhalos have been studied in the literature [78–82]. Here we use $M_{\mathrm{min}} = 10^{-6} M_\odot$ and although there is significant uncertainty on the order of magnitude of M_{min}, the total deposited energy only depends weakly on it.

Obtaining the energy deposited by the halo component of the DM requires performing the same integral as in Eq. (3), over the transfer matrix $T(z', z, E)$. For simplicity, we keep the same parametrization as before, separating out the z–dependence. The total injection power is therefore given by

$$\left(\frac{\mathrm{d}E}{\mathrm{d}t\mathrm{d}V}\right)_{\mathrm{deposited}} = [f(z, m_\chi) + g(z, m_\chi)] \, (1+z)^6 (\Omega_{\mathrm{DM},0} \, \rho_{\mathrm{c},0})^2 \, \zeta \, \frac{\langle\sigma v\rangle}{m_\chi} \; , \tag{5}$$

where $g(z, m_\chi)$, the part of the efficiency factor due to DM halos, is

$$g(z, m_\chi) = \frac{H(z)}{(1+z)^3 \sum_i \int E \frac{\mathrm{d}N}{\mathrm{d}E} \mathrm{d}E} \sum_i \int \mathrm{d}z' \frac{(1+z')^2}{H(z')} \, G(z') \int T_i(z', z, E) \, E \, \frac{\mathrm{d}N}{\mathrm{d}E} \mathrm{d}E \; , \tag{6}$$

and the dimensionless function $G(z)$ is defined as

$$G(z) \equiv \frac{1}{(\Omega_{\mathrm{DM},0} \, \rho_{c,0})^2} \frac{1}{(1+z)^6} \int \mathrm{d}M \, \frac{\mathrm{d}n(M,z)}{\mathrm{d}M} \int_0^{r_\Delta} \mathrm{d}r \, 4\pi r^2 \, \rho_{\mathrm{halo}}^2(r) \; . \tag{7}$$

We also provide a parametrization of the function $g(z, m_\chi)$ for the case of DM annihilation into e^+e^- pairs in Appendix B.

III. COSMOLOGICAL SIGNATURES OF DM ANNIHILATIONS

The electromagnetic energy released by DM annihilations would be deposited into the IGM, inducing heating as well as ionizations and excitations of hydrogen and helium atoms. Excited atoms have a certain probability of being subsequently ionized [83]. Nevertheless, in this work we do not consider this extra source of ionization, which is expected to have a relatively weak effect, of the order of $\sim 10\%$ [21, 22]. In order to compute the changes in the ionization history we use the CosmoRec package [18, 84–89] that includes a subroutine that modifies the evolution equations for the IGM temperature and for the net ionization rate from the ground states of neutral hydrogen and
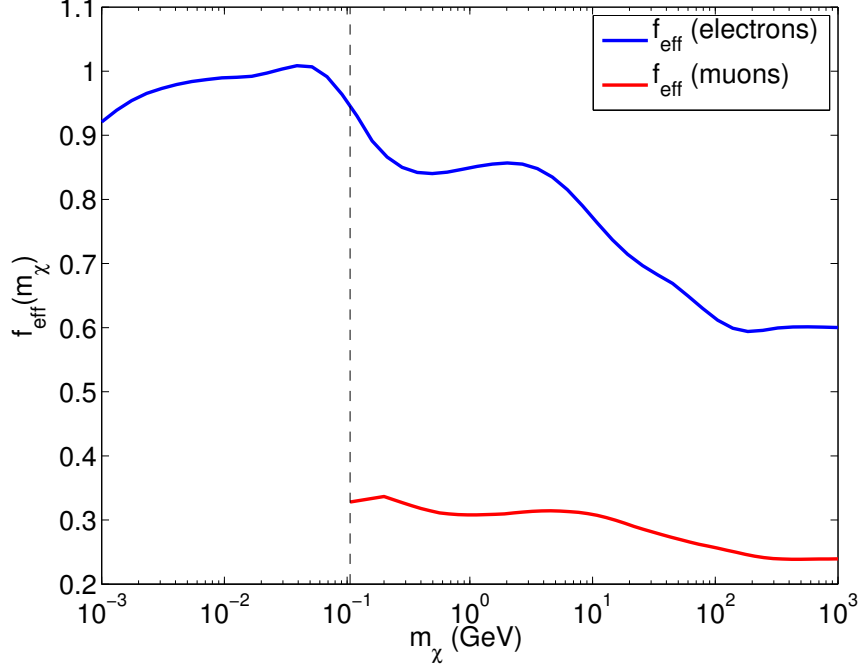
FIG. 1. *The effective energy deposition fractions for the smooth DM background component, as a function of the DM mass, in GeV. Blue (upper) and red (lower) curves denote the e^+e^- and $\mu^+\mu^-$ annihilation channels explored in this study. Red (lower) curve stop at the muon mass, the threshold DM mass for muon production via annihilation.*

helium as

$$\left.\frac{\mathrm{d}T_\mathrm{m}}{\mathrm{d}z}\right|_\mathrm{DM} = -\frac{1}{(1+z)\,H(z)}\frac{2}{3k_\mathrm{B}}\frac{\chi_\mathrm{h}(z)}{N_\mathrm{H}(z)\,[1+f_\mathrm{He}+x_\mathrm{e}(z)]}\left(\frac{\mathrm{d}E}{\mathrm{d}t\mathrm{d}V}\right)_\mathrm{deposited} ; \tag{8}$$

$$\left.\frac{\mathrm{d}x_\mathrm{p}}{\mathrm{d}z}\right|_\mathrm{DM} = \frac{1}{(1+z)\,H(z)}\frac{1}{N_\mathrm{H}(z)\,[1+f_\mathrm{He}]}\frac{\chi_\mathrm{p}(z)}{E_\mathrm{ion}^\mathrm{HI}}\left(\frac{\mathrm{d}E}{\mathrm{d}t\mathrm{d}V}\right)_\mathrm{deposited} ; \tag{9}$$

$$\left.\frac{\mathrm{d}x_\mathrm{HeII}}{\mathrm{d}z}\right|_\mathrm{DM} = \frac{1}{(1+z)\,H(z)}\frac{f_\mathrm{He}}{N_\mathrm{H}(z)\,[1+f_\mathrm{He}]}\frac{\chi_\mathrm{He}(z)}{E_\mathrm{ion}^\mathrm{HeI}}\left(\frac{\mathrm{d}E}{\mathrm{d}t\mathrm{d}V}\right)_\mathrm{deposited} , \tag{10}$$

where T_m is the IGM temperature, $x_\mathrm{p} \equiv N_\mathrm{p}/N_\mathrm{H}$ ($x_\mathrm{HeII} \equiv N_\mathrm{HeII}/N_\mathrm{H}$) is the fraction of ionized atoms from the ground states of neutral hydrogen (helium) relative to the total number of hydrogen nuclei $N_\mathrm{H}(z)$, $f_\mathrm{He} \equiv N_\mathrm{He}/N_\mathrm{H} = 0.0795$ is the fraction of helium nuclei, $x_\mathrm{e} \equiv N_\mathrm{e}/N_\mathrm{H} \simeq x_\mathrm{p} + x_\mathrm{HeII}$ is the free electron fraction, k_B is the Boltzmann constant and $E_\mathrm{ion}^\mathrm{HI} = 13.6$ eV and $E_\mathrm{ion}^\mathrm{HeI} = 24.6$ eV are the ionization potentials for hydrogen and helium, respectively. The specific contributions to the fraction of injected energy converted to ionization from hydrogen and helium are given by $\chi_\mathrm{H}(z)$ and $\chi_\mathrm{He}(z)$ and that converted into heat is $\chi_\mathrm{h}(z)$. It has been shown that for a neutral plasma the amount of energy that goes into heat, ionization and excitation is roughly the same, whereas if it is fully ionized all the energy gets converted into heat [90]. This suggested a simple approximation [1], further refined by including the ionization of helium [4],

$$\chi_\mathrm{h}(z) \approx \frac{1 + 2\,x_\mathrm{p}(z) + f_\mathrm{He}(1 + 2\,Z_\mathrm{HeII}(z))}{3\,(1+f_\mathrm{He})} = \frac{1}{3}\left(1 + 2\,\frac{x_\mathrm{e}(z)}{1+f_\mathrm{He}}\right) ; \tag{11}$$

$$\chi_\mathrm{p}(z) \approx \frac{1 - x_\mathrm{p}(z)}{3} , \tag{12}$$

$$\chi_\mathrm{He}(z) \approx \frac{1 - Z_\mathrm{HeII}(z)}{3} . \tag{13}$$

where $Z_\mathrm{HeII} = N_\mathrm{HeII}/N_\mathrm{He}$ is the fraction of singly ionized helium atoms relative to the total number of helium nuclei.

Now, with these modifications to the evolution equations due to DM annihilations, we can define an effective energy deposition efficiency $f_\mathrm{eff}(m_\chi)$ (for the contribution from the smooth DM component) in order to bypass the
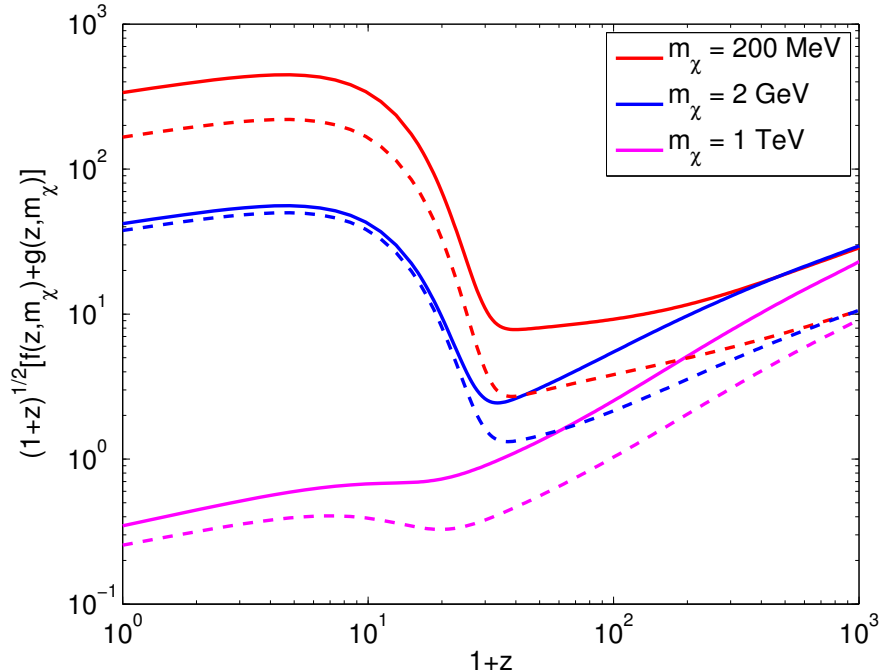
FIG. 2. *The redshift–dependence of the extra contribution to heating and ionization due to DM annihilation, $\sqrt{1+z}\,[f(z,m_\chi)+g(z,m_\chi)]$, for three values of the DM mass (from top to bottom, $m_\chi = 200$ MeV, 2 GeV and 1 TeV). Solid lines are for $\chi\chi \to e^+e^-$ and dashed lines for the $\chi\chi \to \mu^+\mu^-$ channel. The steep rise at low redshifts is due to halo formation.*

computationally expensive interpolation at each redshift of $f(z,m_\chi)$ in our Monte Carlo analyses,

$$f_{\rm eff}(m_\chi) = \frac{\displaystyle\int_{z_{\rm max}}^{z_{\rm min}} f(z,m_\chi)\sqrt{1+z}\,{\rm d}z}{\displaystyle\int_{z_{\rm max}}^{z_{\rm min}} \sqrt{1+z}\,{\rm d}z} \quad , \tag{14}$$

and it parametrizes the effective value of $f(z,m_\chi)$ through the history of the Universe. The factor $\sqrt{1+z}$ is motivated by the redshift dependence of Eqs. (8)–(10), which contain the terms $n_{\rm DM}^2 \propto (1+z)^6$, $N_{\rm H}^{-1} \propto (1+z)^{-3}$ and $((1+z)H(z))^{-1} \sim (1+z)^{-5/2}$ (in the matter–dominated regime). The lower limit for integration is set at $z_{\rm min} = 50$, before reionization starts and the upper limit is chosen to be $z_{\rm max} = 1100$, when the effect of DM annihilations starts to delay recombination[5]. We have verified that the results obtained with the effective deposition efficiency $f_{\rm eff}(m_\chi)$ differ by less than a few percent from those obtained with the full redshift–dependent $f(z,m_\chi)$.

Fig. 1 shows $f_{\rm eff}(m_\chi)$ for DM annihilations into e^+e^- and $\mu^+\mu^-$, as a function of the DM mass. We note that the effective $f_{\rm eff}(m_\chi)$ deposition efficiency is much lower for the $\chi\chi \to \mu^+\mu^-$ channel due the large fraction of final–state neutrinos, which do not heat the IGM nor contribute to ionization. As noted in Section II, $f(z,m_\chi)$ and hence $f_{\rm eff}(m_\chi)$, is larger than 1 for a certain mass range ($m_\chi \sim 100$ MeV) due to a "pile–up" effect: photons and electrons/positrons emitted at early times into their transparency window are eventually redshifted enough to efficiently deposit their energy at later times. Conversely, energy injected from DM particles with masses in the GeV–TeV region will remain in the "transparency window" until the present time lowering the $f_{\rm eff}(m_\chi)$ injection efficiency.

In addition to $f_{\rm eff}(m_\chi)$, we also use an approximation for $g(z,m_\chi)$ so that the $z-$ and m_χ–dependences are factored out,

$$g_{\rm eff}(z,m_\chi) = \gamma(m_\chi)\,\Gamma(z) \tag{15}$$

The fitted functions $\gamma(m_\chi)$ and $\Gamma(z)$ are qualitatively similar to the shape of $f_{\rm eff}(m_\chi)$, and are given in Appendix B.

---

[5] We have checked that using $z_{\rm min} < 50$ or $z_{\rm max} > 1100$ only changes our results by a few percent.
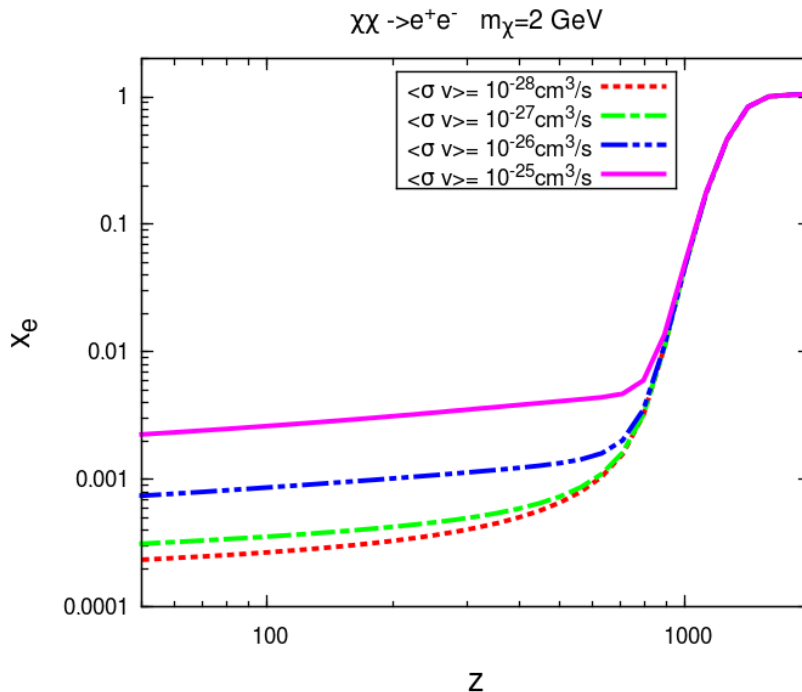
FIG. 3. *Free electron fraction, $x_e(z)$, as a function of the redshift z, for $m_\chi = 2$ GeV and DM annihilations into an e^+e^- pair for different values of the annihilation cross section.*

The total deposited energy that goes into the ionization equations is therefore

$$\left(\frac{\mathrm{d}E}{\mathrm{d}t\mathrm{d}V}\right)_{\mathrm{deposited}} = \left(f_{\mathrm{eff}}(m_\chi) + g_{\mathrm{eff}}(z, m_\chi)\right)\left(\frac{\mathrm{d}E}{\mathrm{d}t\mathrm{d}V}\right)_{\mathrm{injected}} . \tag{16}$$

Once this is taken into account, the redshift–dependence of the extra ionization and heating terms becomes: $\sim \sqrt{1+z}\,[f(z, m_\chi) + g(z, m_\chi)]$. This function is shown for three values of m_χ in Fig. 2.

The main effect of the extra injection of energy from DM annihilations is the delay in recombination at $z \sim 1100$ and an enhancement in the low–redshift tail of the ionization fraction. This modifies the optical depth for CMB photons as they travel from the last scattering surface to us, so that the visibility function, the probability that a photon last scattered at a given redshift, extends to lower redshifts. This changes the position of the acoustic peaks in the temperature power spectrum and broadens the surface of last scattering, suppressing perturbations on scales smaller than the width of this surface and thus attenuates the power spectrum. In addition, the amplitude of the polarization fluctuations is increased and the positions of the TE and EE peaks are shifted, whereas at smaller scales these power spectra are attenuated, similarly to what happens for the temperature power spectrum (see, e.g., Refs [1, 4]).

The impact of annihilating DM on the CMB spectrum is thus an integrated effect which lasts from the early recombination era (high redshift, $z \sim 1100$) until the reionization epoch at late times (low redshift, $z \lesssim 10$). In the early recombination period the presence of the extra heating and ionization terms from DM annihilation processes would change the free electron fraction below $z \sim 1100$. This is depicted in Fig. 3, where we have chosen a DM mass of $m_\chi = 2$ GeV for illustration. When including the effects from the annihilation of DM, the optical depth due to Thomson scattering increases, broadening the last scattering surface and producing a damping of the acoustic oscillations. Although this effect is degenerate with the slope and amplitude of the primordial perturbations, the polarization spectrum helps disentangle the two effects. A number of studies have placed constraints on the DM masses and annihilating cross sections/decaying rates by analyzing these signatures on the CMB temperature and polarization spectra [1–29].

At late times, annihilating DM in halos may also change the reionization history, leaving an imprint in the large scale polarization spectra. Cosmological constraints arising from the reionization period on annihilating or decaying DM have been computed in Refs. [3, 5, 10–12, 15–17, 20, 22, 24]. Although there have been attempts to explain the reionization of the universe solely by the effect of DM annihilation [8, 10–12, 15, 20, 24], we do not consider such a possibility here. We consider mixed reionization scenarios including reionization from both DM annihilation in halos
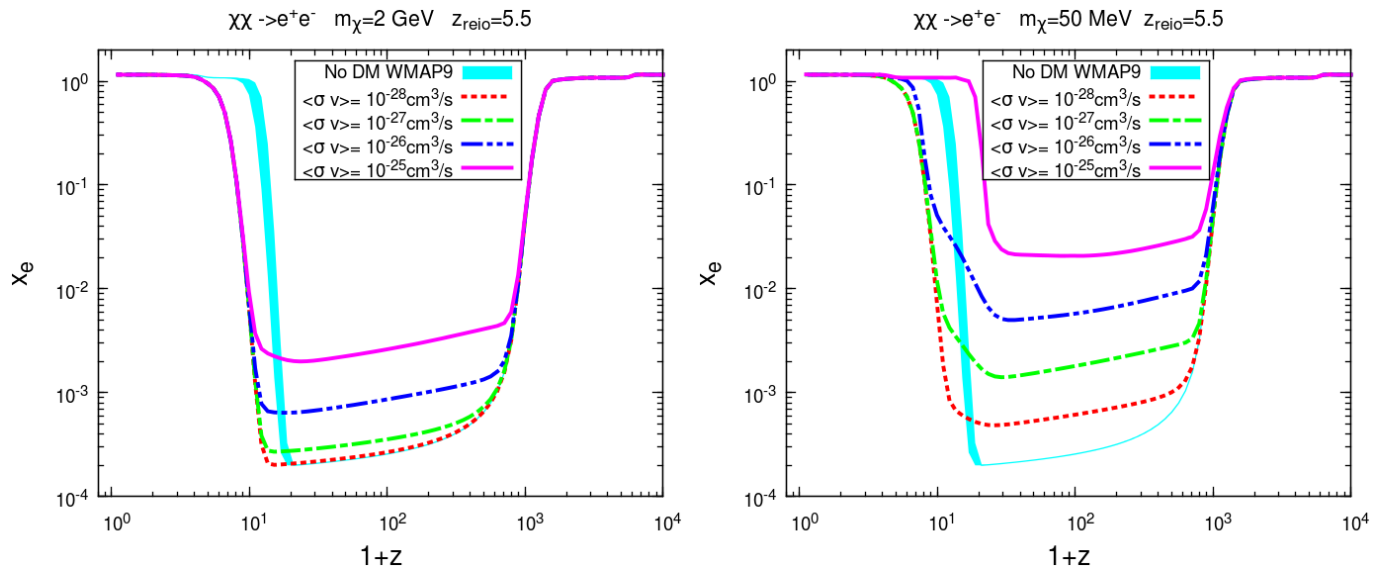
FIG. 4. *Free electron fraction, $x_e(z)$, as a function of the redshift z, in the mixed model explored here, which considers reionization processes from both DM annihilation and first stars. In the left and right panels we depict the cases of DM annihilation into e^+e^- with masses $m_\chi = 2$ GeV and $m_\chi = 50$ MeV, respectively. In these scenarios, the reionization redshift in the CAMB simplified model for the contribution from first stars has been fixed to $z_{\rm reio} = 5.5$. The 1σ error band around the best–fit value from WMAP9 for the case of no contribution from annihilating DM is also plotted.*

and first stars. The latter is accounted for by using the default reionization model implemented in CAMB at a given redshift $z_{\rm reio}$.

The free electron fraction as a function of the redshift for different scenarios with and without DM contribution is depicted in Fig. 4. In both panels, the light blue band shows the WMAP9 1σ error around the best–fit value (in the absence of DM contribution) for the optical depth to reionization $\tau = 0.089 \pm 0.014$. In the left (right) panel of Fig. 4, we consider mixed reionization scenarios with a contribution from the simplified model for reionization from stars at $z_{\rm reio} = 5.5$ plus a contribution from DM particles of $m_\chi = 2$ GeV (50 MeV) annihilating 100% into an e^+e^- pair. We see that the impact of DM contribution on reionization is rather suppressed. In order to get a non-negligible effect we have to consider small masses dark matter masses, such as $m_\chi = 50$ MeV represented here, and annihilation cross sections as large as $\langle \sigma v \rangle = 10^{-25}$ cm^3/s. Given the halo model considered in this work, we can not actually account for the full reionization of the Universe at low redshift with MeV–TeV DM taking into account the bounds on $\langle \sigma v \rangle$ presented below in sec. IV B.

It has also been argued that annihilating DM in halos can increase the reionization optical depth even if reionization by stars occurs at $z \sim 6$, alleviating the tension between the value of the reionization optical depth measured by CMB experiments and the fraction of neutral hydrogen $x_{\rm H} = 1 - x_{\rm p}$ determined by observations of Lyman–α absorption lines in quasar spectra (Gunn–Peterson effect [91]), which require that $x_{\rm H} \geq 10^{-3}$, and perhaps as high as 0.1 at $z \geq 6$ [92, 93] and $x_{\rm H} \leq 10^{-4}$ at $z \leq 5.5$ [92]. This represents an abrupt change of $x_{\rm H}$ (or equivalently x_e) at $z \sim 6$, which cannot be reproduced if $z_{\rm reio} \sim 10$, as indicated by CMB observations. Therefore, and as pointed out in Refs. [8, 10–12, 15, 20, 24], the contribution from DM annihilations in halos could, in principle, explain the measured optical depth by CMB observations, while reionization from the first stars at $z \sim 6$ could complete the reionization process and explain the Gunn–Peterson bounds. However, the value of the annihilation cross section required for this reconciliation is badly excluded by our CMB analyses.

The two panels of Fig. 5 depict the reionization optical depth[6] τ for different values of m_χ as a function of $\langle \sigma v \rangle$ assuming two different values of the redshift of reionization from stars, $z_{\rm reio} = 5.5$ and 10. We also show the 1σ and 2σ bands around the best–fit value for τ from WMAP9 data ($\tau = 0.089 \pm 0.014$) [31]. From both panels, we can see that the larger the DM mass the weaker the constraints on the annihilation cross section, which is the expected behavior (see, e.g., Eq. (1)) due to a smaller number density of DM particles for larger masses. Notice that, for the case of the lower reionization redshift $z_{\rm reio} = 5.5$ (left panel of Fig. 5), as is well known, the optical depth without DM annihilation

---

[6] Notice that in order to compute the reionization optical depth τ, we have integrated between redshift 100 (instead of redshift 40 which is the default value in CAMB) and today.
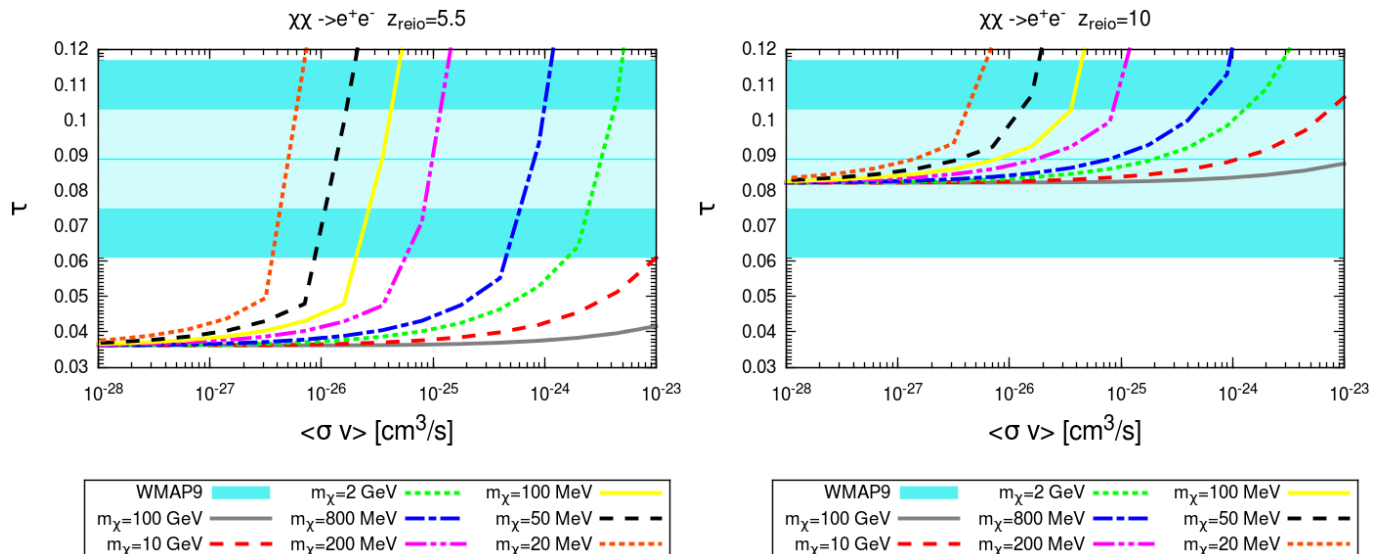
FIG. 5. *Reionization optical depth τ, as a function of the DM annihilation cross section, in the mixed model explored here, which considers reionization processes from both DM annihilation and first stars. We illustrate the behavior for different DM masses assuming 100% annihilation into e^+e^-. In these scenarios, the reionization redshift in the CAMB simplified model for the contribution from first stars has been fixed to $z_{\rm reio} = 5.5$ (left panel) and 10 (right panel). The best–fit value and the 1σ and 2σ error bands from WMAP9 for the case of no contribution from annihilating DM are also shown in light blue.*

would be much lower than the best–fit value measured by the WMAP team, lying three standard deviations away from it. On the other hand, DM masses in the 100's MeV range with cross sections in the $10^{-26}\,{\rm cm}^3{\rm s}^{-1}$ could increase τ to reach the observed value. For the case of $z_{\rm reio} = 10$ (right–hand panel of Fig. 5), DM annihilations in halos are not needed in order to explain the measured value of τ and strong constraints can be placed on the DM annihilation cross section. In our numerical analyses, presented in the following sections, we consider $z_{\rm reio}$ as a free parameter, to be determined by the data.

An additional constraint could arise from Lyman–α observations [16, 24], which appear to indicate that the IGM temperature is a few 10^4 K in the $2 < z < 4.5$ redshift region [94]. Fig. 6 depicts the IGM temperature, $T_{\rm m}$ at redshift $z = 3$ for different values of the annihilating DM mass m_χ versus $\langle\sigma v\rangle$. We indicate as well the value $T_{\rm m} = 32000\,{\rm K}$, that has been considered in Ref. [24] as a conservative upper bound on the IGM temperature at low redshift. The values of $\langle\sigma v\rangle$ that saturate the temperature bound are however several orders of magnitude above the limits that we obtain from CMB data. As a guide for the eye, we reported the latter constraints with brown diamonds in Fig. 6.

IV. ANALYSIS

A. Data and cosmological parameters

In our analyses we explore cosmological scenarios that include DM annihilations and are described by the following set of parameters:

$$\{\omega_{\rm b}, \omega_{\rm DM}, \Theta_{\rm s}, z_{\rm reio}, n_{\rm s}, \log[10^{10}A_{\rm s}], \langle\sigma v\rangle, m_\chi\} , \qquad (17)$$

where $\omega_{\rm b} \equiv \Omega_{\rm b,0}h^2$ and $\omega_{\rm DM} \equiv \Omega_{\rm DM,0}h^2$ are the physical baryon and cold DM energy densities, $\Theta_{\rm s}$ is the ratio between the sound horizon and the angular diameter distance at decoupling, $z_{\rm reio}$ is the reionization redshift, $n_{\rm s}$ is the scalar spectral index, $A_{\rm s}$ is the amplitude of the primordial spectrum, $\langle\sigma v\rangle$ is the thermally–averaged DM annihilation cross section and m_χ is the DM mass. For our numerical analyses, we have used the Boltzmann code CAMB [95]. As explained above, for the recombination calculation and DM contribution to reionization, we have used the CosmoRec package [18, 84–89] since it contains subroutines that account for the additional inputs relevant for the study of DM annihilations. We have then extracted cosmological parameters from current data using a Monte Carlo Markov Chain (MCMC) analysis based on the publicly available MCMC package `cosmomc` [96]. Finally, Table I specifies the priors considered on the different cosmological parameters.
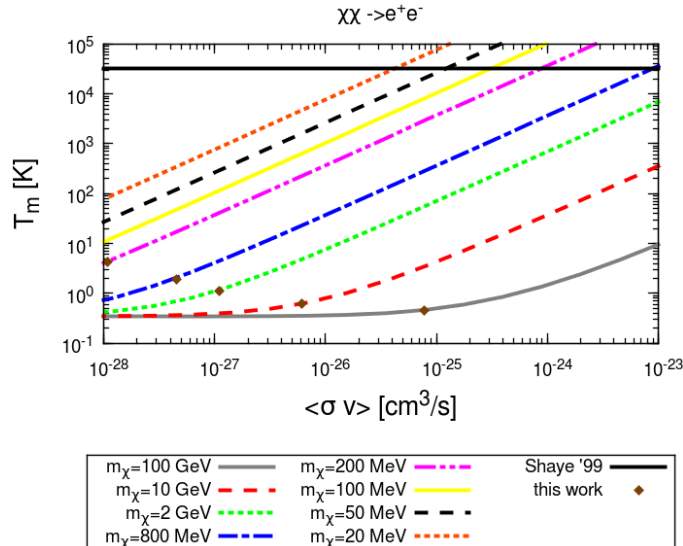
FIG. 6. *IGM temperature T_{m}, in kelvin, as a function of the DM annihilation cross section for different DM masses, assuming that DM annihilation occurs 100% into e^+e^- pairs. The reionization redshift is assumed to be $z_{\mathrm{reio}} = 10$. We indicate the value $T_{\mathrm{m}} = 32000$ K, upper limit from Lyman–α observations for the IGM temperature in the $2 < z < 4.5$ redshift region [94]. We also indicate the upper limit that we obtain for $\langle \sigma v \rangle$ using WMAP9+SPT11+HST+BAO data and the appropriate f_{eff} for each DM mass with brown diamonds.*

Parameter	Prior
$\Omega_{\mathrm{b},0}h^2$	$0.005 \to 0.1$
$\Omega_{\mathrm{DM},0}h^2$	$0.01 \to 0.99$
Θ_{s}	$0.5 \to 10$
z_{reio}	$6 \to 12$
n_{s}	$0.5 \to 1.5$
$\ln\left(10^{10}A_{\mathrm{s}}\right)$	$2.7 \to 4$
$\langle \sigma v \rangle / (3 \cdot 10^{-26}\mathrm{cm}^3/\mathrm{s})$	$10^{-5} \to 10^{2.5}$

TABLE I. *Uniform priors for the cosmological parameters considered here and the DM annihilation cross section.*

Our baseline data set is the WMAP9 data [31] (temperature and polarization) with the routine for computing the likelihood supplied by the WMAP team. Then, we also add CMB data from the SPT'11 [32, 33]. In order to address foreground contributions, the Sunyaev–Zeldovich amplitude, A_{SZ}, the amplitude of the clustered point source contribution, A_{C}, and the amplitude of the Poisson distributed point source contribution, A_{P}, are added as nuisance parameters in the CMB SPT'11 data analysis. Separately, we also consider the most recent high multipole data from the ACT CMB experiment [34] to explore the differences in the constraints on annihilating DM scenarios arising when considering WMAP9 plus either SPT'11 or ACT10 data sets. In addition to the CMB basic data sets, we add the latest constraint on the Hubble constant H_0 from the HST [97] and galaxy clustering measurements, which are considered in our analyses via BAO signals. We use here the BAO signal from DR9 [98] from data of the Baryon Acoustic Spectroscopic Survey (BOSS) [99, 100], with a median redshift of $z = 0.57$. Together with the CMASS DR9 data, we also include the recent measurement of the BAO scale based on a reanalysis (using reconstruction [101]) of the Luminous Red Galaxies (LRG) sample from Data Release 7 with a median redshift of $z = 0.35$ [102], the measurement of the BAO signal at a lower redshift $z = 0.106$ from the 6dF Galaxy Survey (6dFGS) [103] and the BAO measurements from the WiggleZ Survey at $z = 0.44$, $z = 0.6$ and $z = 0.73$ [104].

Dataset		p_{ann} $[10^{-6}$ m^3 s^{-1} kg$^{-1}]$
WMAP7 + ACT'08	(Galli *et al.* [21])	< 1.17
WMAP7 + SPT'09	(Giesen *et al.* [24])	< 0.91
*WMAP7 + SPT'09	this study	< 0.81
WMAP7 + SPT'09		< 0.64
WMAP9 + SPT'09		< 0.44
WMAP9 *only*		< 0.66
WMAP7 + SPT'11		< 0.32
WMAP9 + SPT'11		< 0.27
WMAP9 + ACT'10		< 0.29

TABLE II. *Comparison between this study and previous results of 95% CL limits on p_{ann}, defined in Eq. (18). Our results, labeled "this study" also include HST and BAO data, which were found to have a very small impact on our p_{ann} constraints. All results labeled "this study" were obtained using the priors in Tab. I, except the first line (labeled with an asterisk *) which used the optical depth τ rather than the reionization redshift z_{reio} with priors $\tau \in \{0.01, 0.8\}$. We include this result to facilitate comparison with other studies.*

B. Results

Fig. 7 summarizes our main results in the m_χ–$\langle\sigma v\rangle$ plane and shows the exclusion region extracted from the effect of this type of signatures on the CMB using the most recent observations[7]. The middle solid black line represents the 95% confidence level (CL) exclusion limit for the case of DM annihilations into e^+e^- from the smooth DM background, when analyzing the SPT'11 data set plus WMAP9, BAO and HST, as described above, and using the appropriate $f_{\mathrm{eff}}(m_\chi)$ efficiency function, given in Eq. (14). The dot–dashed blue line shows the equivalent limit using ACT'10 data set plus WMAP9, BAO and HST. The lower solid red curve depicts the analogous 95% CL exclusion limit assuming the energy deposited equals the energy injected ($f(z, m_\chi) = 1$) using WMAP9+SPT'11+HST+BAO data sets. Notice that, when including the effective efficiency $f_{\mathrm{eff}}(m_\chi)$, the $\chi\chi \to e^+e^-$ bounds become less stringent as the DM mass increases compared to those when assuming perfect efficiency ($f(z, m_\chi) = 1$), as expected from the left panel of Fig. 1. Finally, the upper dashed black line illustrates the 95% CL bounds for the $\mu^+\mu^-$ channel, with the corresponding $f_{\mathrm{eff}}(m_\chi)$ function, and using WMAP9+SPT'11+HST+BAO data sets. In this case, the bounds are weaker since $\sim 2/3$ of the energy is lost in the form of neutrinos.

As a comparison with previous studies, we provide the limits on p_{ann}, which is often quoted in the literature, and is defined as:

$$p_{\mathrm{ann}} \equiv f_{\mathrm{eff}}(m_\chi) \frac{\langle\sigma v\rangle}{m_\chi} \ . \tag{18}$$

In Table II we present the bounds illustrated in Fig. 7, as well as our results for WMAP7 data with previous releases of either ACT or SPT data in comparison with some limits from the recent literature. In addition, we show the improvements of individual data sets by adding only one or the other. Tab. II illustrates that while the improvements from the inclusion of HST and BAO priors are marginal, the bounds improve significantly by using more recent CMB data. We attribute part of the difference to the tighter error bars in the WMAP9 polarization data, but find that the our improved bounds are mainly driven by the better accuracy at high ℓ of the recent ACT and SPT data releases.

We find that the inclusion of annihilating DM in halos does not modify the exclusion regions depicted in Fig. 7 for the realistic halo model considered in this work and described in Appendix B. We have recomputed the 95% CL upper bounds, finding no improvement with respect to the bounds obtained when only the contribution from the smooth DM component was considered. The effects of the halo contribution could only be significant with an enhancement of $g(z, m_\chi)$ of at least two orders of magnitude. An increase of about an order of magnitude could be obtained by using a cuspier density profile for the DM halos than NFW. In addition, a decrease by four orders of magnitude in the uncertain and model–dependent minimum halo mass ($M_{\mathrm{min}} = 10^{-10} M_\odot$) would increase the maximum value of $g(z, m_\chi)$ only by a modest factor of ~ 2. Therefore, except from very extreme halo models[8], a large change in $g(z, m_\chi)$

---

[7] Let us note that the best–fit values for the other six cosmological parameters fully agree with the results without DM. For instance, we obtain $z_{\mathrm{reio}} = 10.3 \pm 0.9$ to be compared with $z_{\mathrm{reio}} = 10.6 \pm 1.1$, from WMAP9 [31].

[8] Nevertheless, current N–body simulations can only resolve relatively massive halos at all redshifts (the limiting mass in the simulations we use is $\sim 10^5 M_\odot$ in Ref. [73] and $\sim 10^{12} M_\odot$ at $z = 0$ in Ref. [72]) and hence these results rely on extrapolations to high redshifts and very low mass halos, which are the ones that are expected to contribute the most. In this regard the contribution to the injected energy from DM halos is subject to important uncertainties.
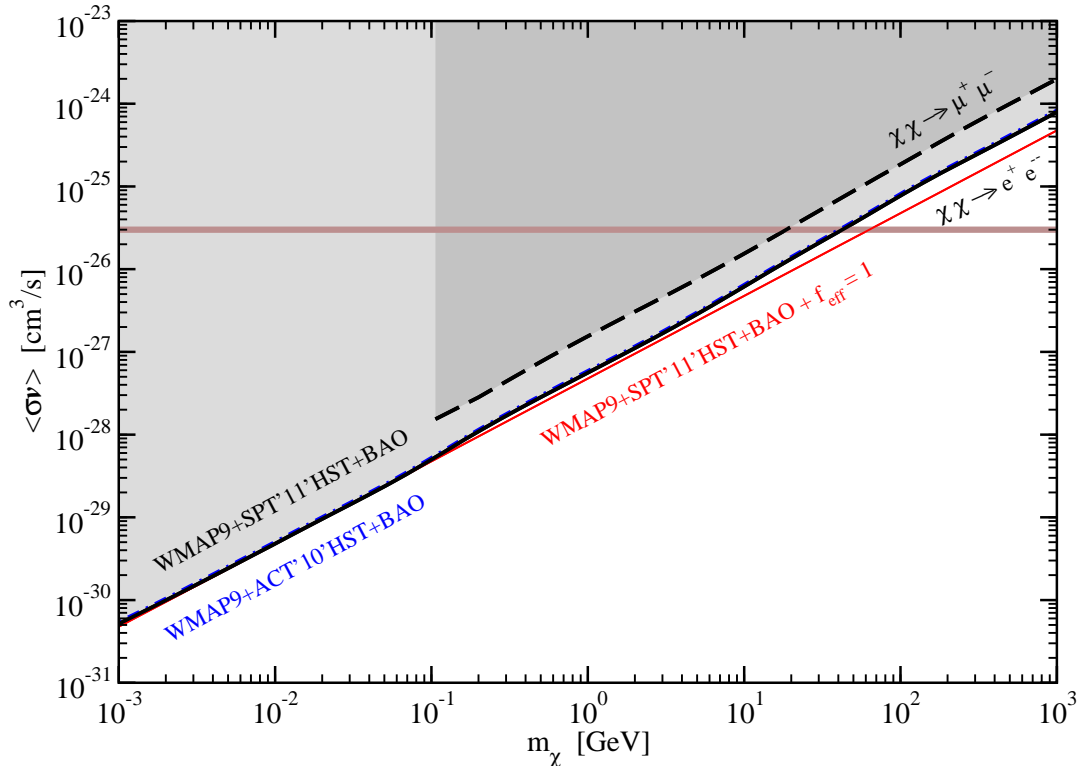
FIG. 7. 95% CL limits on the DM annihilation cross section $\langle\sigma v\rangle$ as a function of the DM mass m_χ for the "SPT" (WMAP9+SPT'11+HST+BAO) and "ACT" (WMAP9+ACT'10+HST+BAO) datasets. The middle solid black (SPT'11) and dot–dashed blue (ACT'10) lines assume an effective deposition efficiency $f_{\rm eff}(m_\chi)$ for $\chi\chi \to e^+e^-$. For the lower solid red line (SPT'11) we assume perfect efficiency, $f(z, m_\chi) = 1$, for $\chi\chi \to e^+e^-$. The upper dashed black line (SPT'11) shows the bounds for $\chi\chi \to \mu^+\mu^-$ with the corresponding effective energy deposition efficiency $f_{\rm eff}(m_\chi)$ for this channel. Note that the results are identical when we include the contribution from DM annihilation in halos as parametrized in this work (see the text). We also show the value of the canonical thermal annihilation cross section, $\langle\sigma v\rangle = 3 \times 10^{-26}{\rm cm}^3{\rm s}^{-1}$.

so that the halo contribution is relevant for CMB constraints, seems difficult to be achieved. Finally, we point out that measurements of the IGM temperature do not further constrain this model (see Fig. 6) and hence the inclusion of a prior on the IGM temperature would not modify the bounds summarized in Fig. 7.

V. CONCLUSIONS

New CMB measurements have recently become available. The WMAP team has released their final nine–year data [31] and new and precise measurements of the CMB damping tail from the SPT [32, 33] and the ACT [34] teams are also publicly available. It is therefore timely to exploit these new cosmological data sets to find bounds on different physics models which may leave signatures on CMB observables.

One of these scenarios is the injection of electromagnetic energy from the annihilations of DM particles from the smooth DM background, which would leave an imprint in both, the temperature and the polarization CMB spectra. After the recombination period, the residual ionization fraction is increased, smearing the visibility function and inducing a damping of the acoustic oscillations. At late times, DM annihilation in halos could also modify the reionization history of the Universe. In this work we have addressed these two effects, by making use of the numerical codes CAMB, CosmoRec and cosmomc to account for and analyze the energy deposited into the CMB by DM annihilation products. For that purpose, we have computed the energy deposition efficiency as a function of the redshift and of the DM particle mass for the case of e^+e^- and $\mu^+\mu^-$ annihilation channels.

We have performed MCMC analyses to the most recent CMB measurements (WMAP9 and separately adding SPT'11 and ACT'10 data sets), along with BAO data and the HST prior on the Hubble constant H_0. We have then computed the mean values and errors of the six "vanilla" parameters in Eq. (17) plus the bounds on the DM annihilation cross section $\langle\sigma v\rangle$ for DM masses ranging from 1 MeV to 1 TeV, which are shown in Fig. 7 and represent

our main result. For instance, with the WMAP9, SPT'11, BAO and HST measurements, we find a 95% CL upper bound of $\langle\sigma v\rangle < 7.3 \cdot 10^{-28}$ cm^3/s for the e^+e^- channel for a DM mass of $m_\chi = 1$ GeV. We exclude the thermal annihilation cross section for masses below 30 GeV for a e^+e^- final state and 15 GeV for the $\mu^+\mu^-$ final state.

Within a mixed reionization scenario, which includes both reionization from first stars plus the contribution to the free electron fraction from DM annihilations in halos (which have been modeled using recent N–body simulations), the constraints from the smooth DM component remain unchanged, even when large uncertainties on the halo model parameters are addressed. Upcoming data from the Planck telescope is expected to improve the current CMB constraints on annihilating/decaying scenarios and a detailed analysis will be carried out elsewhere.

Appendix A: Spectra of injected energy

The simplest case is the direct annihilation to an e^+e^- pair, in which case the electron spectrum is a simple delta function:

$$\frac{\mathrm{d}N_{\mathrm{e}}}{\mathrm{d}y_{\mathrm{e}}} = \delta(1 - y_{\mathrm{e}}) \, , \tag{A1}$$

where $y_{\mathrm{e}} = E_{\mathrm{e}}/m_\chi$. The electron/positron spectrum from the $\chi\chi \to \mu^+\mu^-$ channel (in the limit $m_{\mathrm{e}} \ll m_\mu$) is given by [105]

$$\frac{\mathrm{d}N_{\mathrm{e}}}{\mathrm{d}y_{\mathrm{e}}} = \frac{5}{3} - 3y_{\mathrm{e}}^2 + \frac{4}{3}y_{\mathrm{e}}^3 \, . \tag{A2}$$

In either case, the dominant source of photons from this process comes from internal bremsstrahlung[9] [53, 105]

$$\frac{\mathrm{d}N_\gamma}{\mathrm{d}y_\gamma} = \frac{\alpha}{\pi}\frac{1 + (1 - y_\gamma)^2}{y_\gamma}\left(-1 + \ln\left(\frac{4(1 - y_\gamma)}{\epsilon_\ell}\right)\right), \tag{A3}$$

where $y_\gamma = E_\gamma/m_\chi$ and $\epsilon_\ell = m_\ell/m_\chi$ where $\ell = \{\mathrm{e}, \mu\}$, depending on the annihilation channel.

Note that these expressions represent the spectra per outgoing particle and must be multiplied by 2 to account for the two produced particles per DM annihilation.

Appendix B: Contribution from DM halos to energy deposition

The energy injected into the IGM by DM annihilation in halos at redshift z is given by

$$\left(\frac{\mathrm{d}E}{\mathrm{d}V\mathrm{d}t}\right)_{\mathrm{halo,injected}} = \zeta \, \frac{\langle\sigma v\rangle}{m_\chi} \int \mathrm{d}M \frac{\mathrm{d}n_{\mathrm{halo}}}{\mathrm{d}M}(M, z) \int_0^{r_\Delta} \mathrm{d}r \, 4\pi r^2 \, \rho_{\mathrm{halo}}^2(r) \, , \tag{B1}$$

where the first integral represents the sum of the contributions from all halos and the second integral is the contribution from a single halo.

---

[9] We have neglected the contribution from $\mu \to e \, \nu_e \, \nu_\mu \gamma$, which amounts to corrections to our final results below the percent level.

Let us start by describing the contribution from a halo of mass M. In this term, r_Δ is the radius of a spherical halo at which the mean matter density enclosed within is Δ times the critical density of the Universe at redshift z, $\rho_c(z) = \rho_{c,0} \left(\Omega_m (1+z)^3 + \Omega_\Lambda\right)$, with $\rho_{c,0}$ the critical density at $z=0$, so that the halo mass, M, is

$$M = \Delta\, \rho_c(z)\, \frac{4\pi}{3}\, r_{200}^3 \ . \tag{B2}$$

The injection energy due to DM annihilations depends on the square of the DM density profile. In this work we consider spherical halos with density profiles described by the NFW profile [74],

$$\rho_{\mathrm{halo}}(r) = \rho_s\, \frac{4}{(r/r_s)\,(1+r/r_s)^2} \ , \tag{B3}$$

where r_s is the scale radius and ρ_s the density at that radial distance. Using this profile, the second integral in Eq. (B1) can be computed analytically,

$$\int_0^{r_\Delta} dr\, 4\pi r^2\, \rho_{\mathrm{halo}}^2(r) = \frac{4\pi}{3}\, (4\rho_s)^2\, r_s^3 \left(1 - \frac{1}{(c_\Delta+1)^3}\right)$$
$$= \tilde{g}(c_\Delta)\, \frac{M\,\Delta\,\rho_c(z)}{3} \tag{B4}$$

where we have used the concentration parameter $c_\Delta = r_\Delta/r_s$ and the halo mass M as the parameters defining the density profile, instead of r_s and ρ_s. The function $\tilde{g}(c_\Delta)$ is given by

$$\tilde{g}(c_\Delta) = \frac{c_\Delta^3 \left[1 - (1+c_\Delta)^{-3}\right]}{3\left[\ln(1+c_\Delta) - c_\Delta(1+c_\Delta)^{-1}\right]^2} \ . \tag{B5}$$

It is well known that halo concentrations depend on the halo mass and redshift. Hence, the two–parameter function describing the NFW profile can be reduced to a one–parameter description for each given redshift, and thus Eq. (B4) depends only on M and z.

A parametrization for $c_{200}(M,z)$ using $\sigma(M,z)$ was obtained after a fit of all available data from the Multi-Dark/BigBolshoi simulations[10] [73],

$$c_{200}(M,z) = B_0(x)\, \mathcal{C}(\sigma') \ , \tag{B6}$$

where

$$\mathcal{C}(\sigma') = A\left[\left(\frac{\sigma'}{b}\right)^c + 1\right] \exp\left(\frac{d}{\sigma'^2}\right) \qquad ; \qquad A = 2.881,\ b = 1.257,\ c = 1.022,\ d = 0.060 \tag{B7}$$

and

$$\sigma' = B_1(x)\, \sigma(M,x) \qquad ; \qquad x \equiv \left(\frac{\Omega_{\Lambda,0}}{\Omega_{m,0}}\right)^{1/3} \frac{1}{1+z} \ , \tag{B8}$$

where $\Omega_{m,0}$ is the matter density contribution at $z=0$ and Ω_Λ the contribution to the density from the cosmological constant. The functions $B_0(x)$ and $B_1(x)$ are defined as

$$B_0(x) = \frac{c_{\min}(x)}{c_{\min}(1.393)} \ , \qquad B_1(x) = \frac{\sigma_{\min}^{-1}(x)}{\sigma_{\min}^{-1}(1.393)} \ , \tag{B9}$$

where

$$c_{\min}(x) = c_0 + (c_1 - c_0)\left[\frac{1}{\pi}\arctan\left[\alpha(x - x_0)\right] + \frac{1}{2}\right] \ , \tag{B10}$$

$$\sigma_{\min}^{-1}(x) = \sigma_0^{-1} + (\sigma_1^{-1} - \sigma_0^{-1})\left[\frac{1}{\pi}\arctan\left[\beta(x - x_1)\right] + \frac{1}{2}\right] \tag{B11}$$

---

[10] Note that these simulations have a limited range of validity in halo mass and redshift. Outside this range, we extrapolate the fitting function and set a cutoff on the concentration parameter, $c_{200} = 100$, so that it does not diverge for high redshifts, although the exact value of this cutoff is not important.

with

$$c_0 = 3.681, \; c_1 = 5.033, \; \alpha = 6.948, \; x_0 = 0.424, \tag{B12}$$

and

$$\sigma_0^{-1} = 1.047, \; \sigma_1^{-1} = 1.646, \; \beta = 7.386, \; x_1 = 0.526 \; . \tag{B13}$$

The rms density fluctuation $\sigma(M, z)$ appearing in Eq. (B8) is defined as

$$\sigma^2(M, z) = \left(\frac{D(z)}{D(0)} \right)^2 \int \frac{dk}{k} \frac{k^3 P(k)}{2\pi^2} \left| \tilde{W}(kR) \right|^2 \tag{B14}$$

where $P(k)$ is the linear matter power spectrum and W the Fourier transform of the real–space top–hat window function of radius $R = (3\,M/(4\,\pi\,\rho_{\mathrm{m},0}))^{1/3}$, which is given by $\tilde{W}(kR) = \frac{3}{(kR)^3}\,[\sin kR - (kR)\cos kR]$. A good approximation for $\sigma(M, 0)$ in the range $M \in [10^{-9}, 10^{17}]\,\mathrm{M}_\odot$ is

$$\ln \sigma^{-1}(M, 0) = 0.2506 \left(\frac{M}{\mathrm{M}_\odot} \right)^{0.07536} - 2.6 \left(\frac{M}{\mathrm{M}_\odot} \right)^{0.001745} . \tag{B15}$$

We have obtained $\sigma(M, 0)$ using the linear power spectrum $P(k)$ generated with CAMB package [95] assuming $\Omega_{\mathrm{m}} = 0.27, \Omega_\Lambda = 0.73, h = 0.7, \Omega_{\mathrm{b}} = 0.044$ and $n_{\mathrm{s}} = 0.96$, and then normalized to $\sigma_8 = 0.8$, which were the parameters considered in the N-body simulations in Ref. [72] that we have used in our analysis. We had to continue the spectrum generated by CAMB for $k > 10^4/\mathrm{Mpc}$. For that purpose, we made use of a quadratic fit to $\log[P(\log(k))]$ and k within the $[10, 10^4]/\mathrm{Mpc}$ interval.

The growth factor is defined as

$$D(z) = \frac{5}{2} \left(\frac{\Omega_{\mathrm{m},0}}{\Omega_{\Lambda,0}} \right)^{1/3} \frac{\sqrt{1 + x^3}}{x^{3/2}} \int_0^x \frac{x^{3/2} dx}{[1 + x^3]^{3/2}} \; , \tag{B16}$$

with x given in Eq. (B8), and it can also be approximated as [106, 107]

$$D(z) = \left(\frac{(5/2)\,\Omega_{\mathrm{m}}(z)}{\Omega_{\mathrm{m}}^{4/7}(z) - \Omega_\Lambda(z) + (1 + \Omega_{\mathrm{m}}(z)/2)\,(1 + \Omega_\Lambda(z)/70)} \right) \frac{1}{1 + z} \; , \tag{B17}$$

with $\Omega_{\mathrm{m}}(z) = \Omega_{\mathrm{m},0}(1 + z)^3 / (\Omega_{\mathrm{m},0}(1 + z)^3 + \Omega_\Lambda)$ and $\Omega_\Lambda(z) = 1 - \Omega_{\mathrm{m}}(z)$.

Once the contribution of a single halo is computed, one also needs the halo mass function $\mathrm{d}n_{\mathrm{halo}}/\mathrm{d}M$ (Fig. 8), the number of halos as a function of the halo mass and redshift, which is parametrized as

$$\frac{\mathrm{d}n_{\mathrm{halo}}(M, z)}{\mathrm{d}M} = \frac{\rho_{\mathrm{m}}(z)}{M^2} \frac{\mathrm{d}\ln \sigma^{-1}}{\mathrm{d}\ln M} f(\sigma, z) \; , \tag{B18}$$

where $\rho_{\mathrm{m}}(z) = \rho_{\mathrm{m},0}(1 + z)^3$ is the average matter density at redshift z and $f(\sigma, z)$ is expected to be a universal function[11] with respect to redshift and changes in cosmology and can be parametrized as [108]

$$f(\sigma, z) = A(z) \left[\left(\frac{\sigma}{\beta(z)} \right)^{-\alpha(z)} + 1 \right] e^{-\gamma/\sigma^2} \tag{B19}$$

where[12], for $\Delta = 178$, [72]

$$A_{178}(z) = \Omega_{\mathrm{m}}(z) \left(1.097\,(1 + z)^{-3.216} + 0.074 \right) \; ,$$
$$\alpha_{178}(z) = \Omega_{\mathrm{m}}(z) \left(5.907\,(1 + z)^{-3.599} + 2.344 \right) \; ,$$
$$\beta_{178}(z) = \Omega_{\mathrm{m}}(z) \left(3.136\,(1 + z)^{-3.068} + 2.349 \right) \; ,$$
$$\gamma_{178} = 1.318 \; . \tag{B20}$$

---

[11] We keep the notation $f(\sigma)$ since it is widely used in the literature. It should not be confused with $f(z)$, the energy deposition efficiency from the smooth DM component, which we use throughout the paper.

[12] This parametrization is based on the results obtained in Ref. [72] by using the CubeP^{3}M halofinder (CPMSO) [109] and the Amiga Halo Finder (AHF) [110, 111]. In order to consider the contribution from all halos and at all redshifts, we have to use this fit outside the range where it was obtained, $-0.55 \leq \ln \sigma^{-1} \leq 1.35$ across all redshifts, which at $z = 0$ corresponds to halo masses between $2.6 \times 10^{12}\,\mathrm{M}_\odot$ and $10^{16}\,\mathrm{M}_\odot$. This extrapolation is uncertain and there could be differences of up to a few orders of magnitude with respect to other parametrizations. We have checked that the contribution from halos using the Press-Schechter formalism [69] with a critical linear overdensity for collapse $\delta_{\mathrm{c}} = 1.28$ as used in Refs. [16, 24] (instead of the conventional $\delta_{\mathrm{c}} = 1.686$, or $\delta_{\mathrm{c}} = 1.674$ when considering the influence of dark energy [112–115]) is 2–4 orders of magnitude larger than the parametrization we use, yet remains subdominant with respect to the smooth background contribution.
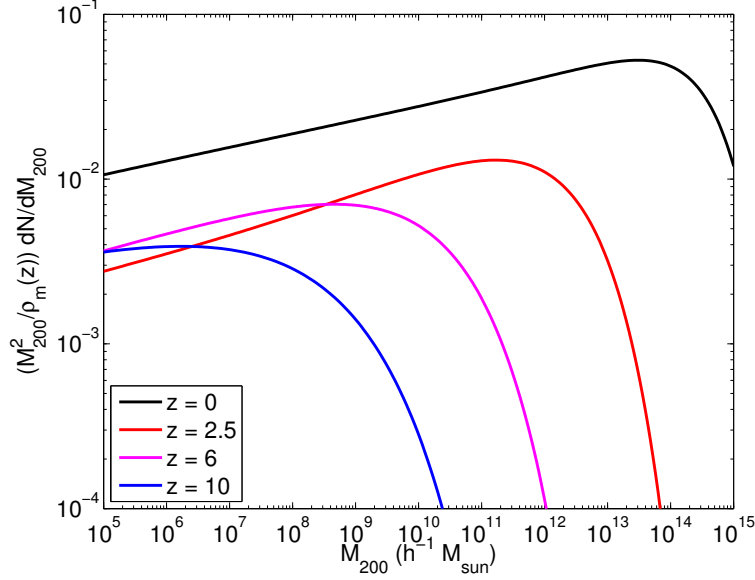
FIG. 8. *The halo mass function* $\mathrm{d}n/\mathrm{d}M(M,z)$ *from the N-body simulations from Ref. [72] at various redshifts, increasing redshift from right to left.*

In order to obtain the result for a different value of Δ, $f(\sigma,z)$ has to be scaled as [72]

$$f_\Delta(\sigma,z) = \left[e^{\left(\frac{\Delta}{178}-1\right)\left(0.023-0.072/\sigma^{2.13}\right)} \left(\frac{\Delta}{178}\right)^{-0.456\,\Omega_{\mathrm{m}}(z)-0.139} \right] f_{178}(\sigma,z) \tag{B21}$$

Hence, Eq. (B1) can be written as

$$\left(\frac{dE}{dV\,dt}\right)_{\mathrm{halo}} = (1+z)^6\,\zeta\,\frac{\langle\sigma v\rangle}{m_\chi}\,\frac{\Delta\,\rho_{\mathrm{m},0}^2}{3\,\Omega_{\mathrm{m}}(z)}\int_{M_{\mathrm{min}}}^\infty \mathrm{d}\log M\,\frac{\mathrm{d}\ln\sigma^{-1}(M,z)}{\mathrm{d}\log M}\,f_\Delta(\sigma(M,z),z)\,\tilde{g}(c_\Delta(M,z))\;. \tag{B22}$$

The function $G(z)$ defined in the text, Eq. (7), is given by

$$G(z) = \left(\frac{\Omega_{\mathrm{m},0}}{\Omega_{\mathrm{DM},0}}\right)^2\,\frac{\Delta}{3\,\Omega_{\mathrm{m}}(z)}\int_{M_{\mathrm{min}}}^\infty \mathrm{d}\log M\,\frac{\mathrm{d}\ln\sigma^{-1}(M,z)}{\mathrm{d}\log M}\,f_\Delta(\sigma(M,z),z)\,\tilde{g}(c_\Delta(M,z))\;, \tag{B23}$$

and we take $\Delta = 200$.

Using this function, one can compute the efficiency $g(z,m_\chi)$, Eq. (6), that can be approximately given by

$$g_{\mathrm{eff}}(z,m_\chi) = \gamma(m_\chi)\,\Gamma(z) \tag{B24}$$

where

$$\ln\gamma(m_\chi) = p_1\,\ln(m_\chi/\mathrm{GeV})^3 + p_2\,\ln(m_\chi/\mathrm{GeV})^2 + p_3\,\ln(m_\chi/\mathrm{GeV}) + p_4\;, \tag{B25}$$
$$\ln\Gamma(z) = q_1(1+z)^{q_2} + q_3(1+z)^{q_4} \tag{B26}$$

with

$$q_1 = -0.008262,\; q_2 = 1.914,\; q_3 = 3.604,\; q_4 = -0.06479\;. \tag{B27}$$

The p_i coefficients for the electron channel are:

$$p_1 = 0.006803,\; p_2 = -0.05783,\; p_3 = -0.8043,\; p_4 = 0.9186\;, \tag{B28}$$

and for the muon channel:

$$p_1 = 0.004854,\; p_2 = -0.05132,\; p_3 = -0.7153,\; p_4 = 0.5491\;, \tag{B29}$$

These approximations do not induce errors larger than a few percent with respect to the case of using the full $g(z, m_\chi)$.

[1] X.-L. Chen and M. Kamionkowski, "Particle decays during the cosmic dark ages", *Phys.Rev.* **D70** (2004) 043502, `arXiv:astro-ph/0310473 [astro-ph]`.

[2] S. H. Hansen and Z. Haiman, "Do we need stars to reionize the universe at high redshifts? Early reionization by decaying heavy sterile neutrinos", *Astrophys.J.* **600** (2004) 26–31, `arXiv:astro-ph/0305126 [astro-ph]`.

[3] E. Pierpaoli, "Decaying particles and the reionization history of the universe", *Phys.Rev.Lett.* **92** (2004) 031301, `arXiv:astro-ph/0310375 [astro-ph]`.

[4] N. Padmanabhan and D. P. Finkbeiner, "Detecting dark matter annihilation with CMB polarization: Signatures and experimental prospects", *Phys.Rev.* **D72** (2005) 023508, `arXiv:astro-ph/0503486 [astro-ph]`.

[5] M. Mapelli, A. Ferrara, and E. Pierpaoli, "Impact of dark matter decays and annihilations on reionzation", *Mon.Not.Roy.Astron.Soc.* **369** (2006) 1719–1724, `arXiv:astro-ph/0603237 [astro-ph]`.

[6] L. Zhang, X.-L. Chen, Y.-A. Lei, and Z.-G. Si, "The impacts of dark matter particle annihilation on recombination and the anisotropies of the cosmic microwave background", *Phys.Rev.* **D74** (2006) 103519, `arXiv:astro-ph/0603425 [astro-ph]`.

[7] E. Ripamonti, M. Mapelli, and A. Ferrara, "Intergalactic medium heating by dark matter", *Mon.Not.Roy.Astron.Soc.* **374** (2007) 1067–1077, `arXiv:astro-ph/0606482 [astro-ph]`.

[8] L. Chuzhoy, "Impact of Dark Matter Annihilation on the High-Redshift Intergalactic Medium", *Astrophys.J.* **679** (2008) L65–L68, `arXiv:0710.1856 [astro-ph]`.

[9] D. P. Finkbeiner, N. Padmanabhan, and N. Weiner, "CMB and 21-cm Signals for Dark Matter with a Long-Lived Excited State", *Phys.Rev.* **D78** (2008) 063530, `arXiv:0805.3531 [astro-ph]`.

[10] A. Natarajan and D. J. Schwarz, "The effect of early dark matter halos on reionization", *Phys.Rev.* **D78** (2008) 103524, `arXiv:0805.3945 [astro-ph]`.

[11] A. Natarajan and D. J. Schwarz, "Dark matter annihilation and its effect on CMB and Hydrogen 21 cm observations", *Phys.Rev.* **D80** (2009) 043529, `arXiv:0903.4485 [astro-ph.CO]`.

[12] A. V. Belikov and D. Hooper, "How Dark Matter Reionized The Universe", *Phys.Rev.* **D80** (2009) 035007, `arXiv:0904.1210 [hep-ph]`.

[13] S. Galli, F. Iocco, G. Bertone, and A. Melchiorri, "CMB constraints on Dark Matter models with large annihilation cross-section", *Phys.Rev.* **D80** (2009) 023505, `arXiv:0905.0003 [astro-ph.CO]`.

[14] T. R. Slatyer, N. Padmanabhan, and D. P. Finkbeiner, "CMB Constraints on WIMP Annihilation: Energy Absorption During the Recombination Epoch", *Phys.Rev.* **D80** (2009) 043526, `arXiv:0906.1197 [astro-ph.CO]`.

[15] G. Hutsi, A. Hektor, and M. Raidal, "Constraints on leptonically annihilating Dark Matter from reionization and extragalactic gamma background", *Astron.Astrophys.* **505** (2009) 999–1005, `arXiv:0906.4550 [astro-ph.CO]`.

[16] M. Cirelli, F. Iocco, and P. Panci, "Constraints on Dark Matter annihilations from reionization and heating of the intergalactic gas", *JCAP* **0910** (2009) 009, `arXiv:0907.0719 [astro-ph.CO]`.

[17] T. Kanzaki, M. Kawasaki, and K. Nakayama, "Effects of Dark Matter Annihilation on the Cosmic Microwave Background", *Prog.Theor.Phys.* **123** (2010) 853–865, `arXiv:0907.3985 [astro-ph.CO]`.

[18] J. Chluba, "Could the cosmological recombination spectrum help us understand annihilating dark matter?", *Mon.Not.Roy.Astron.Soc.* **402** (2010) 1195–1207, `arXiv:0910.3663 [astro-ph.CO]`.

[19] M. Valdes, C. Evoli, and A. Ferrara, "Particle energy cascade in the Intergalactic Medium", *Mon.Not.Roy.Astron.Soc.* **404** (2010) 1569–1582, `arXiv:0911.1125 [astro-ph.CO]`.

[20] A. Natarajan and D. J. Schwarz, "Distinguishing standard reionization from dark matter models", *Phys.Rev.* **D81** (2010) 123510, `arXiv:1002.4405 [astro-ph.CO]`.

[21] S. Galli, F. Iocco, G. Bertone, and A. Melchiorri, "Updated CMB constraints on Dark Matter annihilation cross-sections", *Phys.Rev.* **D84** (2011) 027302, `arXiv:1106.1528 [astro-ph.CO]`.

[22] G. Hutsi, J. Chluba, A. Hektor, and M. Raidal, "WMAP7 and future CMB constraints on annihilating dark matter: implications on GeV-scale WIMPs", *Astron.Astrophys.* **535** (2011) A26, `arXiv:1103.2766 [astro-ph.CO]`.

[23] C. Evoli, M. Valdes, A. Ferrara, and N. Yoshida, "Energy deposition by weakly interacting massive particles: a comprehensiv e study", *Mon.Not.Roy.Astron.Soc.* **422** (2012) 420–433.

[24] G. Giesen, J. Lesgourgues, B. Audren, and Y. Ali-Haimoud, "CMB photons shedding light on dark matter", *JCAP* **1212** (2012) 008, `arXiv:1209.0247 [astro-ph.CO]`.

[25] C. Evoli, S. Pandolfi, and A. Ferrara, "Cosmic microwave background constraints on light dark matter candidates", *Mon.Not.Roy.Astron.Soc.* **433** (2013) 1736–1744, `arXiv:1210.6845 [astro-ph.CO]`.

[26] T. R. Slatyer, "Energy Injection And Absorption In The Cosmic Dark Ages", *Phys.Rev.* **D87** (2012) 123513, `arXiv:1211.0283 [astro-ph.CO]`.

[27] A. R. Frey and N. B. Reid, "Cosmic Microwave Background Constraints on Dark Matter Models of the Galactic Center 511 keV Signal", *Phys.Rev.* **D87** (2013) 103508, `arXiv:1301.0819 [hep-ph]`.

[28] J. M. Cline and P. Scott, "Dark Matter CMB Constraints and Likelihoods for Poor Particle Physicists", *JCAP* **1303** (2013) 044, `arXiv:1301.5908 [astro-ph.CO]`.

[29] C. Weniger, P. D. Serpico, F. Iocco, and G. Bertone, "CMB bounds on dark matter annihilation: Nucleon energy-losses

after recombination", *Phys.Rev.* **D87** (2013) 123008, `arXiv:1303.0942 [astro-ph.CO]`.

[30] C. Dvorkin, K. Blum, and M. Zaldarriaga, "Perturbed Recombination from Dark Matter Annihilation", *Phys. RevD.* **87** (2013) 103522, `arXiv:1302.4753 [astro-ph.CO]`.

[31] **WMAP** Collaboration, G. Hinshaw *et al.*, "Nine-Year Wilkinson Microwave Anisotropy Probe (WMAP) Observations: Cosmological Parameter Results", `arXiv:1212.5226 [astro-ph.CO]`.

[32] **SPT** Collaboration, Z. Hou *et al.*, "Constraints on Cosmology from the Cosmic Microwave Background Power Spectrum of the 2500-square degree SPT-SZ Survey", `arXiv:1212.6267 [astro-ph.CO]`.

[33] **SPT** Collaboration, K. Story *et al.*, "A Measurement of the Cosmic Microwave Background Damping Tail from the 2500-square-degree SPT-SZ survey", `arXiv:1210.7231 [astro-ph.CO]`.

[34] **ACT** Collaboration, J. L. Sievers *et al.*, "The Atacama Cosmology Telescope: Cosmological parameters from three seasons of data", `arXiv:1301.0824 [astro-ph.CO]`.

[35] E. Di Valentino *et al.*, "Tickling the CMB damping tail: scrutinizing the tension between the ACT and SPT experiments", *Phys.Rev.* **D88** (2013) 023501, `arXiv:1301.7343 [astro-ph.CO]`.

[36] E. Calabrese *et al.*, "Cosmological Parameters from Pre-Planck CMB Measurements", *Phys.Rev.* **D87** (2013) 103012, `arXiv:1302.1841 [astro-ph.CO]`.

[37] M. Archidiacono, E. Giusarma, A. Melchiorri, and O. Mena, "Neutrino and Dark Radiation properties in light of latest CMB observations", *Phys.Rev.* **D87** (2013) 103519, `arXiv:1303.0143 [astro-ph.CO]`.

[38] N. Arkani-Hamed, D. P. Finkbeiner, T. R. Slatyer, and N. Weiner, "A Theory of Dark Matter", *Phys.Rev.* **D79** (2009) 015014, `arXiv:0810.0713 [hep-ph]`.

[39] M. Pospelov and A. Ritz, "Astrophysical Signatures of Secluded Dark Matter", *Phys.Lett.* **B671** (2009) 391–397, `arXiv:0810.1502 [hep-ph]`.

[40] I. Cholis, D. P. Finkbeiner, L. Goodenough, and N. Weiner, "The PAMELA Positron Excess from Annihilations into a Light Boson", *JCAP* **0912** (2009) 007, `arXiv:0810.5344 [astro-ph]`.

[41] I. Cholis, G. Dobler, D. P. Finkbeiner, L. Goodenough, and N. Weiner, "The Case for a 700+ GeV WIMP: Cosmic Ray Spectra from ATIC and PAMELA", *Phys.Rev.* **D80** (2009) 123518, `arXiv:0811.3641 [astro-ph]`.

[42] P. Meade, M. Papucci, A. Strumia, and T. Volansky, "Dark Matter Interpretations of the e+- Excesses after FERMI", *Nucl.Phys.* **B831** (2010) 178–203, `arXiv:0905.0480 [hep-ph]`.

[43] F. Chen, J. M. Cline, and A. R. Frey, "Nonabelian dark matter: Models and constraints", *Phys.Rev.* **D80** (2009) 083516, `arXiv:0907.4746 [hep-ph]`.

[44] G. Kane, R. Lu, and S. Watson, "PAMELA Satellite Data as a Signal of Non-Thermal Wino LSP Dark Matter", *Phys.Lett.* **B681** (2009) 151–160, `arXiv:0906.4765 [astro-ph.HE]`.

[45] M. Cirelli, M. Kadastik, M. Raidal, and A. Strumia, "Model-independent implications of the e+-, anti-proton cosmic ray spectra on properties of Dark Matter", *Nucl.Phys.* **B813** (2009) 1–21, `arXiv:0809.2409 [hep-ph]`.

[46] M. Kuhlen, J. Diemand, and P. Madau, "The Dark Matter Annihilation Signal from Galactic Substructure: Predictions for GLAST", *Astrophys.J.* **686** (2008) 262, `arXiv:0805.4416 [astro-ph]`.

[47] J. L. Feng, M. Kaplinghat, and H.-B. Yu, "Sommerfeld Enhancements for Thermal Relic Dark Matter", *Phys.Rev.* **D82** (2010) 083525, `arXiv:1005.4678 [hep-ph]`.

[48] J. M. Cline, A. C. Vincent, and W. Xue, "Leptons from Dark Matter Annihilation in Milky Way Subhalos", *Phys.Rev.* **D81** (2010) 083512, `arXiv:1001.5399 [astro-ph.CO]`.

[49] A. C. Vincent, W. Xue, and J. M. Cline, "Overcoming Gamma Ray Constraints with Annihilating Dark Matter in Milky Way Subhalos", *Phys.Rev.* **D82** (2010) 123519, `arXiv:1009.5383 [hep-ph]`.

[50] C. Boehm, D. Hooper, J. Silk, M. Casse, and J. Paul, "MeV dark matter: Has it been detected?", *Phys.Rev.Lett.* **92** (2004) 101301, `arXiv:astro-ph/0309686 [astro-ph]`.

[51] D. Hooper *et al.*, "Possible evidence for MeV dark matter in dwarf spheroidals", *Phys.Rev.Lett.* **93** (2004) 161302, `arXiv:astro-ph/0311150 [astro-ph]`.

[52] C. Boehm and Y. Ascasibar, "More evidence in favour of light dark matter particles?", *Phys.Rev.* **D70** (2004) 115013, `arXiv:hep-ph/0408213 [hep-ph]`.

[53] J. F. Beacom, N. F. Bell, and G. Bertone, "Gamma-ray constraint on Galactic positron production by MeV dark matter", *Phys.Rev.Lett.* **94** (2005) 171301, `arXiv:astro-ph/0409403 [astro-ph]`.

[54] Y. Ascasibar, P. Jean, C. Boehm, and J. Knoedlseder, "Constraints on dark matter and the shape of the Milky Way dark halo from the 511-keV line", *Mon.Not.Roy.Astron.Soc.* **368** (2006) 1695–1705, `arXiv:astro-ph/0507142 [astro-ph]`.

[55] J. F. Gunion, D. Hooper, and B. McElrath, "Light neutralino dark matter in the NMSSM", *Phys.Rev.* **D73** (2006) 015011, `arXiv:hep-ph/0509024 [hep-ph]`.

[56] J. F. Beacom and H. Yuksel, "Stringent constraint on galactic positron production", *Phys.Rev.Lett.* **97** (2006) 071102, `arXiv:astro-ph/0512411 [astro-ph]`.

[57] C. Boehm and P. Uwer, "Revisiting Bremsstrahlung emission associated with Light Dark Matter annihilations", `arXiv:hep-ph/0606058 [hep-ph]`.

[58] P. Sizun, M. Casse, and S. Schanne, "Continuum gamma-ray emission from light dark matter positrons and electrons", *Phys.Rev.* **D74** (2006) 063514, `arXiv:astro-ph/0607374 [astro-ph]`.

[59] D. P. Finkbeiner and N. Weiner, "Exciting Dark Matter and the INTEGRAL/SPI 511 keV signal", *Phys.Rev.* **D76** (2007) 083519, `arXiv:astro-ph/0702587 [astro-ph]`.

[60] M. Pospelov and A. Ritz, "The galactic 511 keV line from electroweak scale WIMPs", *Phys.Lett.* **B651** (2007) 208–215, `arXiv:hep-ph/0703128 [HEP-PH]`.

[61] N. Prantzos *et al.*, "The 511 keV emission from positron annihilation in the Galaxy", *Rev.Mod.Phys.* **83** (2011)

10011056, arXiv:1009.4620 [astro-ph.HE].

[62] A. C. Vincent, P. Martin, and J. M. Cline, "Interacting dark matter contribution to the Galactic 511 keV gamma ray emission: constraining the morphology with INTEGRAL/SPI observations", *JCAP* **1204** (2012) 022, arXiv:1201.0997 [hep-ph].

[63] N. Fornengo, R. Lineros, M. Regis, and M. Taoso, "Possibility of a Dark Matter Interpretation for the Excess in Isotropic Radio Emission Reported by ARCADE", *Phys.Rev.Lett.* **107** (2011) 271302, arXiv:1108.0569 [hep-ph].

[64] N. Fornengo, R. Lineros, M. Regis, and M. Taoso, "Cosmological Radio Emission induced by WIMP Dark Matter", *JCAP* **1203** (2012) 033, arXiv:1112.4517 [astro-ph.CO].

[65] N. Fornengo, R. A. Lineros, M. Regis, and M. Taoso, "Galactic synchrotron emission from WIMPs at radio frequencies", *JCAP* **1201** (2012) 005, arXiv:1110.4337 [astro-ph.GA].

[66] D. Hooper, A. V. Belikov, T. E. Jeltema, T. Linden, S. Profumo, and T. R. Slatyer, "The Isotropic Radio Background and Annihilating Dark Matter", *Phys.Rev.* **D86** (2012) 103003, arXiv:1203.3547 [astro-ph.CO].

[67] Y. Yang *et al.*, "The contribution of ultracompact dark matter minihalos to the isotropic radio background", *Phys.Rev.* **D87** (2012) 083519, arXiv:1206.3750 [astro-ph.HE].

[68] J. M. Cline and A. C. Vincent, "Cosmological origin of anomalous radio background", *JCAP* **1302** (2013) 011, arXiv:1210.2717 [astro-ph.CO].

[69] W. H. Press and P. Schechter, "Formation of galaxies and clusters of galaxies by selfsimilar gravitational condensation", *Astrophys.J.* **187** (1974) 425–438.

[70] A. Natarajan, "A closer look at CMB constraints on WIMP dark matter", *Phys.Rev.* **D85** (2012) 083517, arXiv:1201.3939 [astro-ph.CO].

[71] R. K. Sheth and G. Tormen, "Large scale bias and the peak background split", *Mon.Not.Roy.Astron.Soc.* **308** (1999) 119, arXiv:astro-ph/9901122 [astro-ph].

[72] W. A. Watson, I. T. Iliev, A. D'Aloisio, A. Knebe, P. R. Shapiro, and G. Yepes, "The halo mass function through the cosmic ages", *Mon.Not.Roy.Astron.Soc.* **433** (2013) 1230–1245, arXiv:1212.0095 [astro-ph.CO].

[73] F. Prada, A. A. Klypin, A. J. Cuesta, J. E. Betancort-Rijo, and J. Primack, "Halo concentrations in the standard LCDM cosmology", *Mon.Not.Roy.Astron.Soc.* **423** (2012) 3018–3030, arXiv:1104.5130 [astro-ph.CO].

[74] J. F. Navarro, C. S. Frenk, and S. D. M. White, "The Structure of Cold Dark Matter Halos", *Astrophys. J.* **462** (1996) 563, arXiv:astro-ph/9508025.

[75] A. M. Green, S. Hofmann, and D. J. Schwarz, "The First wimpy halos", *JCAP* **0508** (2005) 003, arXiv:astro-ph/0503387 [astro-ph].

[76] A. Loeb and M. Zaldarriaga, "The Small-scale power spectrum of cold dark matter", *Phys.Rev.* **D71** (2005) 103520, arXiv:astro-ph/0504112 [astro-ph].

[77] E. Bertschinger, "The Effects of Cold Dark Matter Decoupling and Pair Annihilation on Cosmological Perturbations", *Phys.Rev.* **D74** (2006) 063509, arXiv:astro-ph/0607319 [astro-ph].

[78] T. Bringmann, "Particle Models and the Small-Scale Structure of Dark Matter", *New J.Phys.* **11** (2009) 105027, arXiv:0903.0189 [astro-ph.CO].

[79] J. M. Cornell and S. Profumo, "Earthly probes of the smallest dark matter halos", *JCAP* **1206** (2012) 011, arXiv:1203.1100 [hep-ph].

[80] P. Gondolo, J. Hisano, and K. Kadota, "The Effect of quark interactions on dark matter kinetic decoupling and the mass of the smallest dark halos", *Phys.Rev.* **D86** (2012) 083523, arXiv:1205.1914 [hep-ph].

[81] L. Pieri, E. Branchini, and S. Hofmann, "Difficulty of detecting minihalos via gamm rays from dark matter annihilation", *Phys.Rev.Lett.* **95** (2005) 211301, arXiv:astro-ph/0505356 [astro-ph].

[82] S. M. Koushiappas, "Proper motion of gamma-rays from microhalo sources", *Phys.Rev.Lett.* **97** (2006) 191301, arXiv:astro-ph/0606208 [astro-ph].

[83] P. Peebles, "Recombination of the Primeval Plasma", *Astrophys.J.* **153** (1968) 1.

[84] J. Chluba and R. Thomas, "Towards a complete treatment of the cosmological recombination problem", *Mon.Not.Roy.Astron.Soc.* **412** (2011) 748–764, arXiv:1010.3631 [astro-ph.CO].

[85] Y. Ali-Haimoud and C. M. Hirata, "Ultrafast effective multi-level atom method for primordial hydrogen recombination", *Phys.Rev.* **D82** (2010) 063521, arXiv:1006.1355 [astro-ph.CO].

[86] J. Chluba, G. Vasil, and L. Dursi, "Recombinations to the Rydberg States of Hydrogen and Their Effect During the Cosmological Recombination Epoch", *Mon.Not.Roy.Astron.Soc.* **407** (2010) 599–612, arXiv:1003.4928 [astro-ph.CO].

[87] D. Grin and C. M. Hirata, "Cosmological hydrogen recombination: The effect of extremely high-n states", *Phys.Rev.* **D81** (2010) 083005, arXiv:0911.1359 [astro-ph.CO].

[88] E. R. Switzer and C. M. Hirata, "Primordial helium recombination. 3. Thomson scattering, isotope shifts, and cumulative results", *Phys.Rev.* **D77** (2008) 083008, arXiv:astro-ph/0702145 [ASTRO-PH].

[89] J. Rubino-Martin, J. Chluba, W. Fendt, and B. Wandelt, "Estimating the impact of recombination uncertainties on the cosmological parameter constraints from cosmic microwave background experiments", *Mon.Not.Roy.Astron.Soc.* **403** (2010) 439–452, arXiv:0910.4383 [astro-ph.CO].

[90] J. M. Shull and M. E. van Steenberg, "X-ray secondary heating and ionization in quasar emission-line clouds", *Astrophys. J.* **298** (1985) 268–274.

[91] J. E. Gunn and B. A. Peterson, "On the Density of Neutral Hydrogen in Intergalactic Space", *Astrophys.J.* **142** (1965) 1633.

[92] X.-H. Fan, C. Carilli, and B. G. Keating, "Observational constraints on cosmic reionization", *Ann.Rev.Astron.Astrophys.* **44** (2006) 415–462, arXiv:astro-ph/0602375 [astro-ph].

[93] J. Caruana, A. J. Bunker, S. M. Wilkins, E. R. Stanway, M. Lacy, M. J. Jarvis, S. Lorenzoni, and S. Hickey, "No Evidence for Lyman-alpha Emission in Spectroscopy of $z > 7$ Candidate Galaxies", *Mon.Not.Roy.Astron.Soc.* **427** (2012) 3055–3070, arXiv:1208.5987 [astro-ph.CO].

[94] J. Schaye, T. Theuns, M. Rauch, G. Efstathiou, and W. L. Sargent, "The Thermal history of the intergalactic medium", *Mon.Not.Roy.Astron.Soc.* **318** (2000) 817, arXiv:astro-ph/9912432 [astro-ph].

[95] A. Lewis, A. Challinor, and A. Lasenby, "Efficient computation of CMB anisotropies in closed FRW models", *Astrophys.J.* **538** (2000) 473–476, arXiv:astro-ph/9911177 [astro-ph].

[96] A. Lewis and S. Bridle, "Cosmological parameters from CMB and other data: A Monte Carlo approach", *Phys.Rev.* **D66** (2002) 103511, arXiv:astro-ph/0205436 [astro-ph].

[97] A. G. Riess, L. Macri, S. Casertano, H. Lampeitl, H. C. Ferguson, A. V. Filippenko, S. W. Jha, L. Weidong, and R. Chornock, "A 3% Solution: Determination of the Hubble Constant with the Hubble Space Telescope and Wide Field Camera 3", *Astrophys.J.* **730** (2011) 119, arXiv:1103.2976 [astro-ph.CO].

[98] **BOSS** Collaboration, L. Anderson *et al.*, "The clustering of galaxies in the SDSS-III Baryon Oscillation Spectroscopic Survey: Baryon Acoustic Oscillations in the Data Release 9 Spectroscopic Galaxy Sample", *Mon.Not.Roy.Astron.Soc.* **428** (2013) 1036–1054, arXiv:1203.6594 [astro-ph.CO].

[99] **BOSS** Collaboration, D. Schlegel *et al.*, "The Baryon Oscillation Spectroscopic Survey: Precision measurements of the absolute cosmic distance scale", arXiv:0902.4680 [astro-ph.CO].

[100] **BOSS** Collaboration, K. S. Dawson *et al.*, "The Baryon Oscillation Spectroscopic Survey of SDSS-III", *Astron.J.* **145** (2013) 10, arXiv:1208.0022 [astro-ph.CO].

[101] D. J. Eisenstein, H.-J. Seo, E. Sirko, and D. Spergel, "Improving Cosmological Distance Measurements by Reconstruction of the Baryon Acoustic Peak", *Astrophys.J.* **664** (2007) 675–679, arXiv:astro-ph/0604362 [astro-ph].

[102] N. Padmanabhan, X. Xu, D. J. Eisenstein, R. Scalzo, A. J. Cuesta, K. T. Mehta, and E. Kazin, "A 2% Distance to $z = 0.35$ by Reconstructing Baryon Acoustic Oscillations - I : Methods and Application to the Sloan Digital Sky Survey", *Mon.Not.Roy.Astron.Soc.* **427** (2012) 2132–2145, arXiv:1202.0090 [astro-ph.CO].

[103] F. Beutler, C. Blake, M. Colless, D. H. Jones, L. Staveley-Smith, L. Campbell, Q. Parker, W. Saunders, and F. Watson, "The 6dF Galaxy Survey: Baryon Acoustic Oscillations and the Local Hubble Constant", *Mon.Not.Roy.Astron.Soc.* **416** (2011) 3017–3032, arXiv:1106.3366 [astro-ph.CO].

[104] C. Blake *et al.*, "The WiggleZ Dark Energy Survey: mapping the distance-redshift relation with baryon acoustic oscillations", *Mon.Not.Roy.Astron.Soc.* **418** (2011) 1707–1724, arXiv:1108.2635 [astro-ph.CO].

[105] J. Mardon, Y. Nomura, D. Stolarski, and J. Thaler, "Dark Matter Signals from Cascade Annihilations", *JCAP* **0905** (2009) 016, arXiv:0901.2926 [hep-ph].

[106] O. Lahav, P. B. Lilje, J. R. Primack, and M. J. Rees, "Dynamical effects of the cosmological constant", *Mon.Not.Roy.Astron.Soc.* **251** (1991) 128–136.

[107] S. M. Carroll, W. H. Press, and E. L. Turner, "The Cosmological constant", *Ann.Rev.Astron.Astrophys.* **30** (1992) 499–542.

[108] J. L. Tinker, A. V. Kravtsov, A. Klypin, K. Abazajian, M. S. Warren, G. Yepes, S. Gottlober, and D. E. Holz, "Toward a halo mass function for precision cosmology: The Limits of universality", *Astrophys.J.* **688** (2008) 709–728, arXiv:0803.2706 [astro-ph].

[109] J. Harnois-Deraps, U.-L. Pen, I. T. Iliev, H. Merz, J. Emberson, *et al.*, "High Performance P3M N-body code: CUBEP3M", arXiv:1208.5098 [astro-ph.CO].

[110] S. P. Gill, A. Knebe, and B. K. Gibson, "The Evolution substructure 1: A New identification method", *Mon.Not.Roy.Astron.Soc.* **351** (2004) 399, arXiv:astro-ph/0404258 [astro-ph].

[111] S. R. Knollmann and A. Knebe, "Ahf: Amiga's Halo Finder", *Astrophys.J.Suppl.* **182** (2009) 608–624, arXiv:0904.3662 [astro-ph.CO].

[112] P. B. Lilje, "Abundance of rich clusters of galaxies: A test for cosmological parameters", *Astrophys. J. Lett.* **386** (1992) L33–L36.

[113] S. D. White, G. Efstathiou, and C. Frenk, "The Amplitude of mass fluctuations in the universe", *Mon.Not.Roy.Astron.Soc.* **262** (1993) 1023–1028.

[114] C. S. Kochanek, "Gravitational lensing limits on cold dark matter and its variants", *Astrophys.J.* **453** (1995) 545, arXiv:astro-ph/9411082 [astro-ph].

[115] V. R. Eke, S. Cole, and C. S. Frenk, "Using the evolution of clusters to constrain Omega", *Mon.Not.Roy.Astron.Soc.* **282** (1996) 263–280, arXiv:astro-ph/9601088 [astro-ph].